DEUTSCHES ELEKTRONEN-SYNCHROTRON

DESY 94-160
September 1994


# Recent Results from *ep* Scattering at HERA

T. Haas

*Deutsches Elektronen-Synchrotron DESY, Hamburg*

Representing the H1 and ZEUS Collaboration

ISSN 0418-9833

NOTKESTRASSE 85 - 22603 HAMBURG

To be sure that your preprints are promptly included in the
HIGH ENERGY PHYSICS INDEX,
send them to (if possible by air mail):

| | |
|---|---|
| **DESY**<br>**Bibliothek**<br>**Notkestraße 85**<br>**22603 Hamburg**<br>**Germany** | **DESY-IfH**<br>**Bibliothek**<br>**Platanenallee 6**<br>**15738 Zeuthen**<br>**Germany** |

DESY 94-160
September 1994

ISSN 0418-9833

# Recent Results from *ep* Scattering at HERA *

Presented for the H1 and ZEUS Collaborations by
**Tobias Haas**
*Deutsches Elektronen Synchrotron (ZEUS Collaboration)*
*Notkestrasse 85, 22603 Hamburg, Germany*

**Abstract**

The HERA experiments, H1 and ZEUS, had their second running period during the summer and fall of 1993 collecting 0.5 $pb^{-1}$ of data each, a twentyfold increase in statistics over the previous running period. This large increase in statistics together with an improved understanding of the detectors has brought a wide range of physics questions within the reach of the experiments. In this report we give a brief overview of some of the studies performed recently.

## 1 Introduction

From May through October 1993 the two detector collaborations H1 and ZEUS at the HERA electron-proton collider at DESY in Hamburg had their second data-taking period. During that period HERA delivered over 1 $pb^{-1}$ of luminosity for each experiment, twenty times more than during the first run in 1992. This increase in statistics permits a wide range of investigations in a kinematic range inaccessible to previous fixed target experiments. The following highlights of the experimental programme are described in this report:

- the measurement of the total $\gamma p$ cross section at center-of-mass energies around 200 GeV;
- the separation of elastic, diffractive and non-diffractive components of the $\gamma p$ interactions;

*Talk given at the PASCOS 94 conference in Syracuse, N. Y..



- the observation of exclusive vector meson production both in quasi-real photoproduction ($Q^2 \sim 0$ GeV$^2$) and deep inelastic scattering ($Q^2 > 4$ GeV$^2$);
- the observation of direct and resolved interactions of the photon with the proton;
- the measurement of the gluon component in the photon;
- the measurement of the proton structure function $\mathcal{F}_2$ in the range $4 < Q^2 < 10^4$ GeV$^2$;
- the measurement of the charged current cross section in a totally new kinematic regime;
- the measurement of the strong coupling constant $\alpha_S$ from the two-jet rate in deep-inelastic scattering (DIS); and,
- the observation of large-rapidity-gap events in DIS.

## 2 Experimental setup

### 2.1 *HERA machine conditions*

The two experiments, H1 and ZEUS, are located at the electron-proton collider HERA at DESY in Hamburg. During 1993 HERA operated with bunches of electrons of energy $E_e = 26.7$ GeV colliding with bunches of protons of energy $E_p = 820$ GeV, with a time between bunch crossings of 96 ns. HERA is designed to run with 210 bunches in each of the electron and proton rings. For the 1993 data-taking, 84 paired bunches were filled for each beam and in addition 10 electron and 6 proton bunches were left unpaired for background studies. The electron and proton beam currents were typically 10 mA. The design currents are 58 mA for electrons and 163 mA for protons.

### 2.2 *The H1 and ZEUS detectors*

A detailed description of the H1 and ZEUS detectors can be found in [1] and [2, 3]. Here we give a brief overview of the two detectors concentrating on those parts which were used for the analyses shown here. Schematic views of the detectors are shown in Figs. 1 and 2. Both H1 and ZEUS are multipurpose detectors with slightly different emphases: H1 focuses on the optimal reconstruction of the scattered electrons in high $Q^2$ neutral-current deep-inelastic-scattering events with excellent energy and angle resolution in their electromagnetic calorimeter. ZEUS, on the other hand, has a compensating hadron calorimeter in order to optimally measure the hadronic final state in addition to measuring the scattered electron.

In the case of H1 a tracking system consisting of jet chambers and multiwire proportional chambers surrounds the interaction point. The resolutions in the plane perpendicular to the beam direction range from 250 $\mu$m for the innermost to 580 $\mu$m in the outermost chambers. In the forward direction the resolution in the $R\phi$-plane is enhanced by a radial chamber with a resolution of 290 $\mu$m. The resolution along the beam direction is enhanced by two $Z$-chambers with resolutions of 250 $\mu$m and 340 $\mu$m respectively. The tracking system together with the liquid argon calorimeter are arranged inside a superconducting coil with a diameter of about

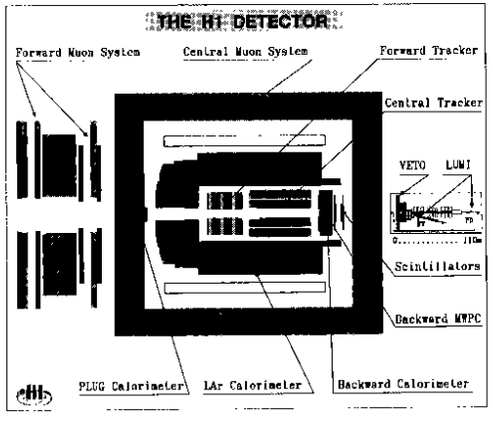


Figure 1: Schematic view of the H1 detector.

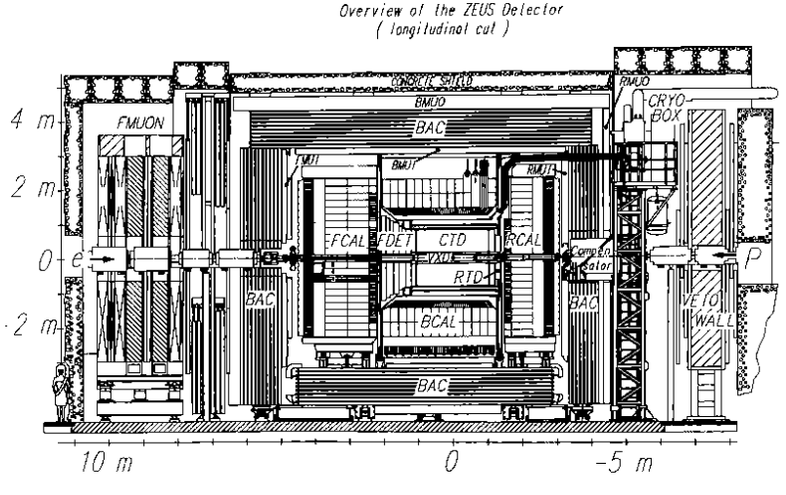


Figure 2: Schematic view of the ZEUS detector.



6 m providing a homogeneous longitudinal magnetic field of 1.2 T. The coil is placed outside the calorimeter to minimize the amount of dead material in front of the calorimeter.

In the case of ZEUS charged particles are tracked by two inner tracking detectors: The vertex detector (VXD) immediately surrounding the beampipe is a cylindrical drift chamber with a resolution of 50 $\mu$m in the central region of a drift cell and 150 $\mu$m near the edges [4]. Surrounding the VXD is the central drift chamber (CTD) consisting of 72 cylindrical drift chamber layers [5]. The CTD currently achieves a resolution of 260 $\mu$m in the $R\phi$-plane. A homogeneous axial magnetic field of 1.42 T is provided by a superconducting coil which immediately surrounds the tracking system.

In both H1 and ZEUS the tracking systems are enclosed by electromagnetic and hadronic calorimeters. H1 uses liquid argon with lead absorbers in the electromagnetic sections and steel absorbers in the hadronic sections [6]. This system extends over the pseudorapidity[1] range $3.4 > \eta > -1.4$ and its energy resolution is $\sigma_E/E \approx 0.12/\sqrt{E[GeV]} \oplus 0.01$ for electrons and $\sigma_E/E \approx 0.50/\sqrt{E[GeV]} \oplus 0.02$ for charged pions, as determined under testbeam conditions. The backward region of the detector, $-1.35 > \eta > -3.6$, is closed by a lead-scintillator calorimeter (BEMC) with a depth of 22.5 radiation lengths. It is used predominantly to trigger and measure the scattered electrons in DIS processes with $Q^2$ ranging from 5 to 100 GeV$^2$. The BEMC achieves a resolution of $\sigma_E/E = 0.10/\sqrt{E[GeV]} \oplus 0.42/E[GeV] \oplus 0.03$.

In ZEUS the solenoid immediately surrounds the tracking system followed by the high-resolution uranium-scintillator calorimeter on the outside. The ZEUS calorimeter is divided into three parts, forward (FCAL) covering the pseudorapidity region $4.3 \geq \eta \geq 1.1$, barrel (BCAL) covering the central region $1.1 \geq \eta \geq -0.75$ and rear (RCAL) covering the backward region $-0.75 \geq \eta \geq -3.8$. Holes of $20 \times 20$ cm$^2$ in the center of FCAL and RCAL accommodate the HERA beam pipe. The resulting solid angle coverage is 99.7% of $4\pi$. The calorimeter parts are subdivided into towers which in turn are subdivided longitudinally into electromagnetic (EMC) and hadronic (HAC) sections. The sections are subdivided into cells, each of which is viewed by two photomultiplier tubes. The ZEUS calorimeter is described in detail in [7].

Both experiments also include detectors to measure the luminosity and to tag electrons scattered at very small angles. These devices consist of two electromagnetic calorimeters located upstream of the interaction points with respect to the proton direction in HERA. They measure the bremsstrahlung photons emitted at very small angles in the interaction region together with the radiating electrons. In ZEUS lead-scintillator calorimeters are placed at 35 m and 107 m to detect electrons and photons, respectively [8]. In H1 the arrangement is similar.

# 3 Photoproduction

The $ep$ total cross section is dominated by interactions where the virtuality of the exchanged photon is very small ($Q^2 \sim 0$) and the photon can therefore be regarded as an almost-real particle. The high center-of-mass energy available at HERA permits the study of the physics of these almost-real photons at energies up to $W_{\gamma p} = 250$ GeV. In the rest frame of the proton this corresponds to photon energies of up to 20 TeV.

[1] The pseudorapidity $\eta$ is defined as $-\ln(\tan\frac{\theta}{2})$ where the polar angle $\theta$ is taken with respect to the proton beam direction from the nominal interaction point.

| Experiment | Process | $< W_{\gamma p} >$ | $\sigma_{\gamma p}$ |
|---|---|---|---|
| H1 | Total | 197 GeV | $156 \pm 2(stat) \pm 18(sys)\mu$b |
| ZEUS | Total | 180 GeV | $143 \pm 4(stat) \pm 17(sys)\mu$b |
| ZEUS | Non diffractive | 180 GeV | $64.0 \pm 0.9 \pm 3.6\%$ of Total |
| ZEUS | Inelastic diffractive | 180 GeV | $23.3 \pm 1.4 \pm 4.7\%$ of Total |
| ZEUS | Elastic | 180 GeV | $12.7 \pm 2.7 \pm 4.3\%$ of Total |

Table 1: Photoproduction cross sections from H1 [10] and ZEUS [11].

### 3.1 Total cross section

Two types of event samples are used to study photoproduction events: the tagged sample is obtained by measuring the scattered electron emerging from the interaction with reduced energy but practically undeflected. The untagged sample is obtained by explicitly looking for events with no scattered electron in the main detector but significant hadronic activity in the calorimeter. For the tagged events the inelasticity, $y$, is then determined from the energies of the incoming and outgoing electrons, $E_e$ and $E'_e$, through

$$y = 1 - \frac{E'_e}{E_e}. \tag{1}$$

For untagged events one has only the information from the hadronic system in the detector to find $y$ according to the method of Jacquet and Blondel [9],

$$\delta_H = \sum_i E_i(1 - \cos\theta_i), \tag{2}$$

$$y = \frac{\delta_H}{2E_e}. \tag{3}$$

Here the sum runs over all calorimeter cells and $E_i$ and $\theta_i$ are the energies and polar angles of the individual calorimeter cells as seen from the interaction vertex.

One extracts the total photoproduction cross section, $\sigma^{\gamma p}_{tot}$, from the measured electroproduction cross section using

$$\frac{d\sigma^{ep}}{dy} = \frac{\alpha}{2\pi}\left[\frac{1+(1-y)^2}{y}\cdot \ln\left(\frac{Q^2_{max}}{Q^2_{min}}\right) - \frac{2(1-y)}{y}\cdot\left(\frac{Q^2_{max}}{Q^2_{min}}\right)\right]\cdot \sigma^{\gamma p}_{tot}(W_{\gamma p}). \tag{4}$$

In this formula $Q^2_{max}$ and $Q^2_{min}$ depend on the detector acceptance and are typically $10^{-2}$ and $10^{-8}$ GeV$^2$. Taking only the first term in the square brackets gives the well known Weizsäcker-Williams approximation.

The measured cross sections from both H1 and ZEUS are given in Table 1. These results together with lower energy data are also shown in Fig. 3. As can be seen, the total cross section displays a very small rise or constant behavior with energy, well compatible with parametrizations inspired by Regge-type analyses such as DL [12] and ALLM [13]. Calculations including QCD hard scattering [14] predict a steeper rise of the cross section. However, within the present measurement error the curve labeled "minijets" in Fig. 3, which is one such calculation with a minimum $p_t = 2$ GeV, is also compatible with the data.



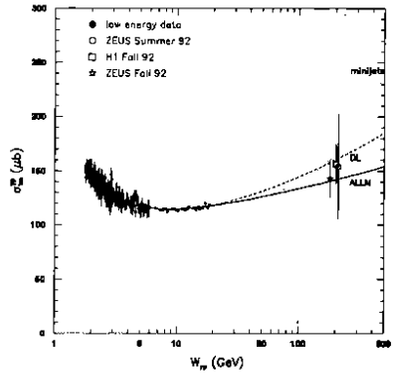


Figure 3: The total photoproduction cross section as a function of the $\gamma p$ center-of-mass energy, $W_{\gamma p}$. The solid line is the prediction of the ALLM parametrization, the dashed line is that of DL and the dotted line is a QCD calculation which includes hard scattering.

### 3.2 Exclusive vector meson production

Photoproduced vector mesons have been extensively studied in fixed target experiments up to center-of-mass energies of about $W_{\gamma p} = 20$ GeV. HERA extends the energy range for these studies by almost one order of magnitude. The photoproduction of vector mesons is usually described in terms of the vector meson dominance model (VMD) [15]. In this model the photon fluctuates into a hadron with the quantum numbers of the photon, typically a $\rho$ meson, which elastically scatters off the proton. The behaviour of the scattering amplitudes for these types of processes can be explained in terms of the exchange of a colourless object, often referred to as the pomeron. At some energy scale this picture should merge into a perturbative description where, however, it is not clear what variable sets the scale.

Fig. 4 compares the total photoproduction cross section as a function of $W$ with several partial cross sections for the low energy data and the HERA data. In particular the cross sections for elastic vector meson production, ($\rho$, $\omega$ and $\phi$) and for the elastic production of J/$\psi$ are shown. Currently HERA measurements exist for $\gamma p \to \rho p$ and $\gamma p \to \psi p$. The measured cross sections are [16, 17, 18]

$$\begin{aligned}
\textbf{ZEUS}: &\quad \sigma^{\gamma p\to\rho p}(60 < W_{\gamma p} < 80 \text{ GeV}) &&= 12.5 \pm 0.7(stat.) \pm 2.8(sys.)\mu\text{b},\\
\textbf{ZEUS}: &\quad \sigma^{ep\to\psi ep}(40 < W_{\gamma p} < 140 \text{ GeV}, \mu^+\mu^- mode) &&= 6.7 \pm 1.2(stat.) \pm 2.0(sys.)\text{nb},\\
\textbf{ZEUS}: &\quad \sigma^{ep\to\psi ep}(40 < W_{\gamma p} < 140 \text{ GeV}, e^+e^- mode) &&= 7.4 \pm 1.2(stat.) \pm 1.6(sys.)\text{nb},\\
\textbf{H1}: &\quad \sigma^{ep\to\psi ep}(30 < W_{\gamma p} < 180 \text{ GeV}, l^+l^- modes) &&= 8.8 \pm 2.0(stat.) \pm 2.2(sys.)\text{nb}.
\end{aligned}$$

An inclusive measurement of the elastic production of light vector mesons from ZEUS yields [11]

$$\sigma^{\gamma p\to V p}(W = 180 \text{ GeV}) = 18 \pm 7\mu\text{b}. \tag{5}$$

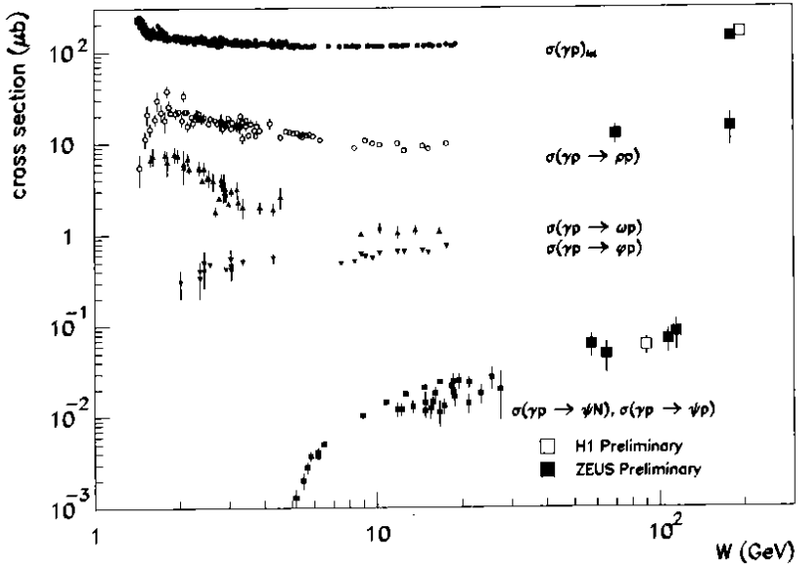


Figure 4: The total photoproduction cross section, $\sigma^{tot}$, as a function of $W_{\gamma p}$ compared to cross sections for the elastic production of $\rho$, $\omega$, $\phi$ and J/$\psi$. HERA results exist for the total cross section, the process $\gamma p \to \rho p$ and $\gamma p \to \psi p$. The large solid squares are the ZEUS results and the large open squares are the H1 results.



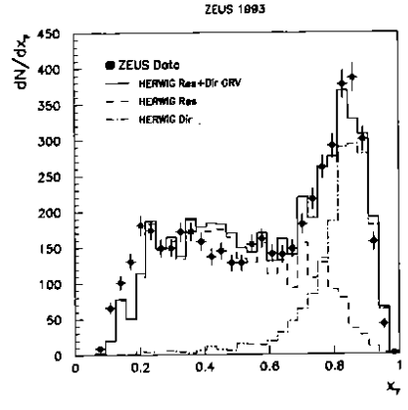


Figure 5: Distribution of $x_\gamma$ measured by the ZEUS detector. The data are not corrected for detector acceptance. In particular, the method used to reconstruct $x_\gamma$ does not allow values $> 1$. below $x_\gamma = 0.1$ the distribution is cut off by rejecting jets in the very forward part of the detector.

### 3.3 Hard scattering and the gluon in the photon

At HERA energies the interactions between almost real photons (i.e. with virtuality $Q^2 \sim 0$) may produce jets with high transverse energy. The presence of a 'hard' energy scale means that perturbative QCD should be applicable to the experimental data. To leading order, $\mathcal{O}(\alpha_S)$, two processes are responsible for jet production. The photon may interact as a point-like particle with a parton in the proton, or it may first fluctuate into an hadronic state. In the first case, known as the direct contribution, the hadronic final state consists of two jets and the proton remnant. In the second case, known as the resolved contribution, the photon acts as a source of partons which scatter off partons in the proton. In addition to the hard jets and the proton remnant one may then also observe a photon remnant. The two contributions separate in the variable $x_\gamma$, the fraction of the photon momentum flowing into the hard interaction. In events with two hard jets $x_\gamma$ is determined from

$$x_\gamma = \frac{\sum_{jets}(E_i - P_{Zi})}{\sum_{part}(E_i - P_{Zi})}, \tag{6}$$

where the sum in the denominator runs over all particles and the sum in the numerator runs over only those particles assigned to the hard jets. Fig. 5 shows the distribution of $x_\gamma$ for two-jet events in photoproduction with $E_T^{jet} > 6$ GeV from the ZEUS experiment [19]. The $\gamma p$ center-of-mass energy, $W_{\gamma p}$, ranges between 132 and 265 GeV. The peak near $x_\gamma = 1$, stemming from the direct contribution, can be clearly distinguished from the part which rises toward smaller values of $x_\gamma$ (below $x_\gamma = 0.1$ the distribution is cut off since jets in the very forward part of the detector have been excluded). This latter part stems from the resolved contribution.

From the measured distribution of $x_\gamma$ one can extract an effective gluon density in the photon. The gluonic component in the photon should become dominant at values of $x_\gamma < 0.1$. As $x_\gamma$

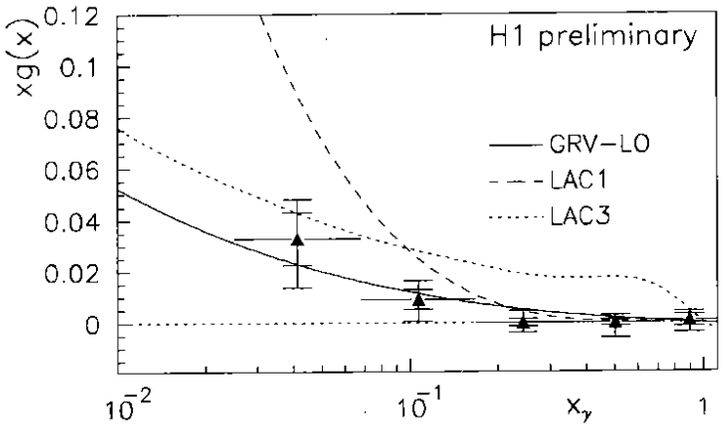


Figure 6. Effective gluon parton distribution in the photon, as determined by the H1 collaboration.

decreases the hard jets go more and more into the foward direction and get entangled with the proton remnant, complicating the measurement. A first attempt by the H1 Collaboration [20] to measure in this region is shown in Fig. 6. Here the effective gluon density in the photon has been extracted from a measurement extending down to $x_\gamma \approx 10^{-2}$ and unfolding back to the partonic level. The systematic errors are large but one sees first indications that, just as in the case of the proton (see discussion in the next section), the gluon density in the photon might be growing rapidly at low values of $x_\gamma$. Also shown with the data is the prediction for the gluon density by Glück, Reya and Vogt (GRV-LO) [21] and two parametrizations by Levy, Abramowicz and Charchula (LAC1 and LAC3) [22] which predict such a rise. However, a distinction between different parametrizations is not yet possible.

# 4 Deep inelastic scattering

In deep-inelastic neutral-current scattering (DIS), to lowest order, the space-like photon with momentum $q$ and virtuality $Q^2 = -q^2$ is absorbed by a parton in the proton carrying a fraction $x = Q^2/(2P \cdot q)$ of the proton's momentum $P$ and producing a single jet in the final state in addition to the proton remnant. This picture is modified in higher order where multiple gluons may be radiated off the incoming or outgoing parton lines. HERA covers a new kinematic regime with momentum transfers $Q^2$ ranging to $10^5$ GeV$^2$ and the fractional parton momentum in the proton, $x$, as low as $5 \cdot 10^{-5}$ for $Q^2$-values above 4 GeV$^2$. The detectors have high resolution and hermetic hadron calorimeters permitting precise measurements of the hadronic final states in this new kinematic range.



## 4.1 The structure function $\mathcal{F}_2$ of the proton

The measurement of the proton structure functions is one of the central investigations at HERA. Therefore it is covered in more detail in a separate contribution to this conference by Dau [23]. Here we give only a very brief summary of the results.

The double differential cross section for neutral-current deep-inelastic $ep$ scattering is given in terms of the structure functions $\mathcal{F}_i$ by:

$$\frac{d^2\sigma_{NC}}{dxdQ^2} = \frac{2\pi\alpha^2}{xQ^4}\left[Y_+\mathcal{F}_2(x,Q^2) - y^2\mathcal{F}_L(x,Q^2) + Y_-x\mathcal{F}_3(x,Q^2)\right] \quad (7)$$

where $Y_\pm = 1 \pm (1-y)^2$. Currently at HERA only the structure function $\mathcal{F}_2$ is measured. The contributions from $\mathcal{F}_L$, the longitudinal part, and $\mathcal{F}_3$, the parity-violating part arising from $Z^o$ exchange, are maximally $< 20\%$, but typically much less, and are input from QCD calculations. Fig. 7 shows the HERA results for the structure function $\mathcal{F}_2$ of the proton as a function of $Q^2$ at different values of $x$. The logarithmic scaling violations become clearly visible at low values of $x$. The scaling violations are a direct consequence of QCD and it is possible to extract the gluon density from them [23]. Another important property of the data is the strong rise of $\mathcal{F}_2$ at low $x$. This had been reported previously [24] and is now corroborated with much improved precision.

## 4.2 Charged current cross section

At HERA one can study the reaction $ep \to \nu_e + hadrons$ in a high energy kinematic regime where the $W$ propagator plays an important role. In particular, the momentum transfer $Q^2$ ranges up to about $10^5$ GeV$^2$ and $< Q^2 >$ becomes comparable to $M_W^2 = (80\ \text{GeV})^2$ causing a substantial deviation from the linear behaviour of the cross section with energy observed in previous neutrino fixed target experiments which studied the inverse reaction.

Fig. 8 shows the first measurement of the charged current cross section at HERA by the H1 experiment [25] which, for the purpose of comparing to the neutrino data, has been extrapolated to low $p_t$ and the corresponding quark flavour couplings. The low energy data have been taken from [26]. One should note that the equivalent fixed target energy of the HERA collider is 50 TeV, two orders of magnitude higher than the highest neutrino experiment.

The deviation from the linear behavior of the cross section is clearly visible showing the sensitivity to the mass of the $W$ propagator. The cross section measured by the H1 experiment is

$$\sigma_{CC}(p_t > 25\ \text{GeV}) \;=\; 55 \pm 15(stat.) \pm 6(sys.)\text{pb}.$$

Fig. 9 shows the dependance of the neutral current, $ep \to e + hadrons$ (solid diamonds), and the charged current, $ep \to \nu_e + hadrons$ (open diamonds), cross sections on the momentum transfer $Q^2$. One sees that the two cross sections become equal at the scale where the electromagnetic and the weak forces are unified. The two lines are the predictions of the Born-level calculations obtained from the Monte Carlo program LEPTO [27]. The predictions are in good agreement with the data.

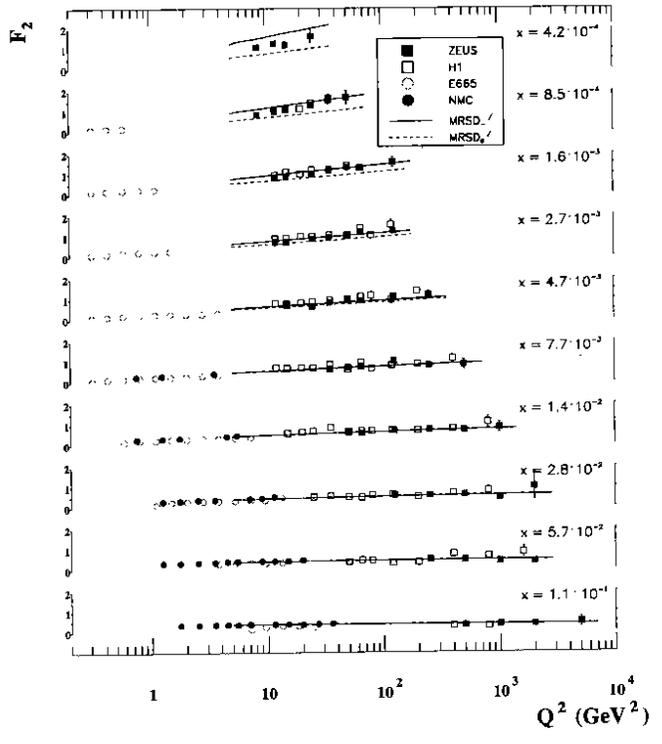


Figure 7: The structure function $\mathcal{F}_2$ of the proton as a function of $Q^2$ at different values of $x$. Note the broken vertical scale.



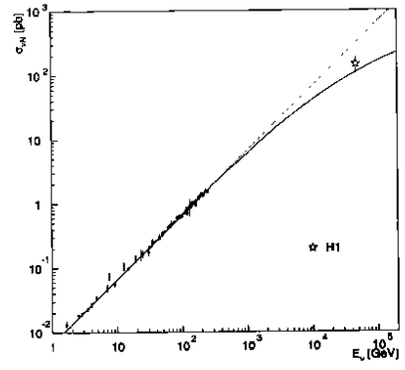


Figure 8: The energy dependence of the $\nu N$ cross section. The crosses represent the low energy neutrino data while the full and the open stars refer to the HERA measurements, which for the purpose of this comparison, have been converted to a $\nu N$ cross section. The H1 point correspond to an equivalent fixed target energy of 50 TeV. The straight line is the extrapolation from low energies assuming $m_W = \infty$ while the curve represents the predicted cross section including the $W$ propagator.

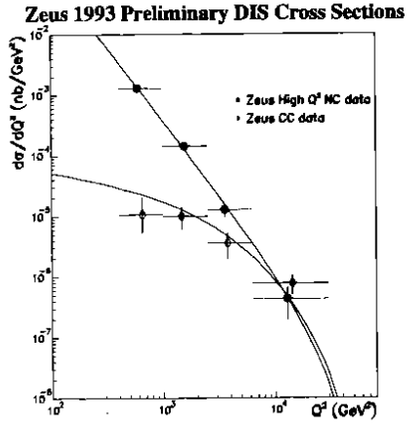


Figure 9: The cross sections $d\sigma/dQ^2$ for neutral and charged current $ep$ interactions. The solid diamonds are the neutral current data and the open diamonds are the charged current data. The two lines are the respective Born-level calculations obtained from the LEPTO Monte Carlo program.

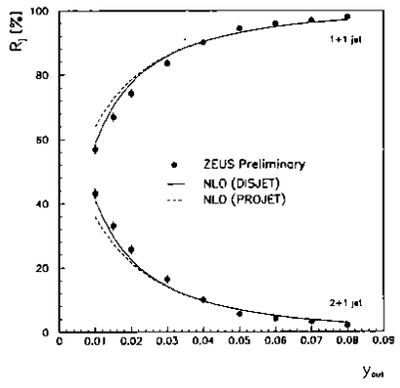


Figure 10: The DIS jet production rates, $R_j$, for 1+1 and 2+1 jets in %, as a function of $y_{cut}$ in the range $160 < Q^2 < 1280$ GeV$^2$, $0.01 < x < 0.1$ and $0.04 < y < 0.95$. The dashed line is the NLO calculation by Graudenz and the solid line is the NLO calculation by Brodkorb and Mirkes.

## 4.3 Two-jet production and $\alpha_S$

The inclusive jet cross section in DIS is dominated by 1+1-jet events. Here the "+1" stands for the proton remnant. QCD processes, e.g. final state gluon radiation, lead to additional jets in the final state. At the high center-of-mass energy available at HERA one can easily observe these multi-jet events [28, 29]. These events cannot be explained by the naïve Quark-Parton Model. In particular, they can be used to measure parameters of QCD such as the strong coupling constant, $\alpha_S$. $\alpha_S$ of course runs with the scale at which it is probed. At HERA the measurement of $\alpha_S(Q^2)$ can in principle extend over the full kinematic range accessible to the experiments up to values of $10^5$ GeV$^2$. HERA therefore presents a laboratory in which to test the running of $\alpha_S$ over a very large range.

In order to perform such a measurement one needs to relate hadron jets to QCD partons with the help of jet algorithms. Here we present results obtained with JADE-type clustering algorithms since currently theoretical calculations exist only for these algorithms [30, 31]. The distance measure used is a scaled invariant mass,

$$y_{ij} = \frac{2E_iE_j(1-\cos\theta_{ij})}{W^2}, \qquad (8)$$

where $E_i$ and $E_j$ are the particle energies, $\theta_{ij}$ is the polar angle between the particles and $W^2$ is the squared invariant mass of the hadronic final state. These algorithms cluster particles until the distance between any two clusters becomes larger than some resolution cutoff, $y_{cut}$. For DIS processes at HERA a pseudoparticle carrying the missing longitudinal momentum is added to account for the proton beam remnant. Fig. 10 shows the rates, $R_j = N_{j+1}/(N_{1+1}+N_{2+1})$, of 1+1 and 2+1-jet events in the range $160 < Q^2 < 1280$ GeV$^2$, $0.01 < x < 0.1$ and $0.04 < y < 0.95$ as a function of this cutoff measured by the ZEUS experiment [32]. The rate is compared



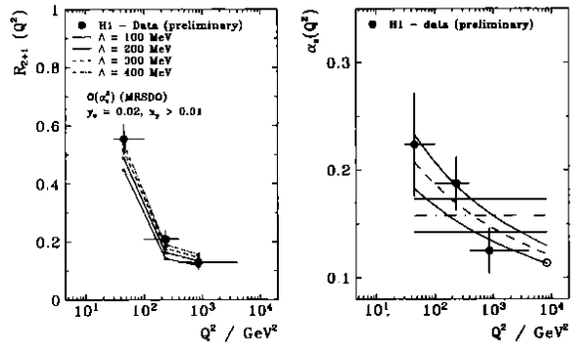


Figure 11:
**a:** The 2+1-jet rate as a function of $Q^2$ at $y_{cut} = 0.2$ in the range $x > 0.01$. Also shown are the predictions from the NLO calculation obtained from the PROJET Monte Carlo program.
**b:** The strong coupling constant $\alpha_S(Q^2)$ extracted from the three points in (a) and then fitted to the 2-loop solution of the renormalization group equation (dashed line with corresponding error band). Also shown is a constant value of $\alpha_S$ (dash-dotted lines). The open circle is the average value measured from jet rates at LEP [33].

to two analytic calculations by Graudenz [30] and Brodkorb and Mirkes [31]. A value of $\Lambda^{(5)}_{\overline{MS}} = 312$ MeV was chosen in this comparison, corresponding to $\alpha_S(M_Z^2) = 0.124$, a value which has been measured from jet rates in $e^+e^-$ annihilations [33]. This shows that jet rates measured at HERA are in good quantitative agreement with the $e^+e^-$ results.

Going one step further, one can fix the resolution parameter and study the 2+1-jet rate as a function of $Q^2$ and, since this rate is known to $\mathcal{O}(\alpha_S^2)$, extract the strong coupling constant. Fig. 11 shows the result of this measurement from the H1 experiment [20] for a value of $y_{cut} = 0.02$. Also shown are the predictions from PROJET [30] at different values of the QCD scale, $\Lambda_{QCD}$. The data favor the running of $\alpha_S$ over a constant value.

## 4.4 Large-rapidity-gap events in DIS

In general, the hadronic final state in DIS events is characterized by a large energy deposition in between the forward direction (with respect to the proton direction) and the direction of the quark jet. This energy presumably stems from gluons radiated in the colour field between the outgoing partons and from the proton remnant. However, the HERA experiments have observed a class of DIS events with a gap in the hadronic activity between the proton remnant and the most forward hadron seen in the detector [34, 35]. The effect is seen in Fig. 12 which shows the distribution of the variable $\eta_{max}$, the pseudorapidity of the most forward energy deposition in the calorimeter above 400 MeV [34]. Standard DIS Monte Carlo models (e.g. ARIADNE 4.1 [36], solid line) fail to predict an adequate rate of events with values of $\eta_{max} < 1.5$. Models

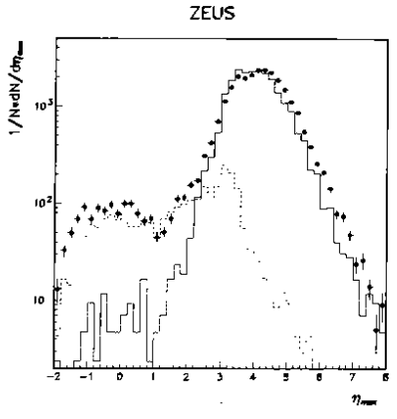


Figure 12: The distribution of the pseudorapidity of the most forward calorimeter cluster for DIS events. The solid circles are the ZEUS data, the solid histogram is the prediction of the ARIADNE Monte Carlo model and the dashed histogram is the prediction of the POMPYT Monte Carlo model.

for diffractive deep-inelastic scattering (e.g. POMPYT [37]) are able to predict a sufficient rate of events with a gap as well as their $\eta_{max}$ distribution.

Studying the inclusive properties of these events, one finds that they are very similar to the standard DIS events [34]. In particular, the rate of large-rapidity-gap events compared to the total DIS rate is approximately constant with $W$, the center-of-mass energy of the $\gamma^* p$ system, and at fixed $x$ it does not depend on $Q^2$. Furthermore, clear jet structures are observed in these events with the jet $E_T$ ranging up to 7 GeV [38]. This indicates that in these events the photon couples to a point-like object inside the proton in much the same way as the photon couples to the partons in "ordinary" DIS events.

Splitting the DIS sample into events with $\eta_{max} > 1.5$, called non-rapidity-gap events, and events with $\eta_{max} < 1.5$, called large-rapidity-gap events, one can compare the hadronic final states of these two event classes. Fig. 13 shows the energy flow as a function of the pseudorapidity difference between the calorimeter cells and the hypothetical direction of the massless quark jet. In the non-rapidity-gap data at high $Q^2$ (open circles in Fig. 13b) on sees a pronounced peak near $\Delta\eta = 0$ stemming from the quark jet. Hadronic activity fills in the entire rapidity range between the struck quark and the proton remnant. At low $Q^2$ (Fig. 13a) the peak from the struck quark is much less pronounced and also shifted towards the proton direction. This effect can be explained as arising from the invariant mass produced by gluon radiation. In the large-rapidity-gap events the peak near $\Delta\eta = 0$ has only a small shift even at low $Q^2$ and its collimation changes little indicating that QCD radiation is suppressed in the large-rapidity-gap events.



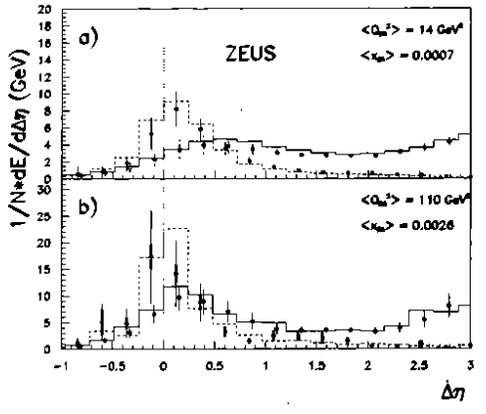


Figure 13: The energy flow distribution, $1/N \cdot dE/d(\Delta\eta)$, as a function of the pseudorapidity difference, $\Delta\eta$, in two bins of $Q^2$. The open circles are the non-rapidity-gap events ($\eta_{max} > 1.5$), the solid circles are the large-rapidity-gap events ($\eta_{max} < 1.5$), the full histogram is the prediction of the Colour Dipole Model (ARIADNE) and the dotted histogram is the prediction of the POMPYT Monte Carlo model.

# 5 Summary and Outlook

The two HERA experiments have collected a total of $\sim 1$ pb$^{-1}$ of data during the 1993 running. This has brought forth a wide range of results in a totally new kinematic region of lepton-proton scattering. From HERA we know now that the proton structure function $\mathcal{F}_2$ rises strongly at low $x$, that the photoproduction cross section is almost constant with energy up to about 200 GeV and that diffraction in $ep$ scattering is not only a soft phenomenon but is observed at high momentum transfers and may be accompanied by hard jets. These are just the highlights among many other interesting results. Yet they open up new questions: does $\mathcal{F}_2$ continue to rise at yet lower $Q^2$ and lower $x$? at what values will it start to saturate and by what mechanism? does the photoproduction cross section start to rise more steeply at some yet higher scale as some theories predict? and last, but not least, how can the hard diffraction processes seen at HERA be described and brought into line with the soft diffraction seen at much lower energies?

All of these questions and many more will be investigated at HERA as the machine reaches its design goals for the luminosity, provides polarized electrons and runs at different energies. The HERA program is indeed a very rich one and we can hope for many more interesting results in the near future.

# References

[1] F. Brasse, Proc. 26th Int. Conf. on High Energy Physics, Dallas, ed. J. R. Sanford (1992) 1849;

H1 Collab., I. Abt et al., "The H1 Detector at HERA", DESY 93-103 (1993).

[2] The ZEUS Detector, Status Report 1993, DESY 1993.

[3] ZEUS Collab., M. Derrick et al., Phys. Lett. B 293 (1992) 465.

[4] C. Alvisi et al., Nucl. Instr. and Meth. A305 (1991) 30.

[5] C. B. Brooks et al., Nucl. Instr. and Meth. A283 (1989) 477;
B. Foster et al., Nucl. Instr. and Meth. A338 (1994) 254.

[6] H1 Calorimeter Group, B. Andrieu et al., Nucl. Inst. and Meth. A336 (1993) 460;
H1 Calorimeter Group, B. Andrieu et al., Nucl. Inst. and Meth. A336 (1993) 499.

[7] A. Andresen et al., Nucl. Inst. and Meth. A309 (1991) 101;
A. Caldwell et al., Nucl. Inst. and Meth. A321 (1992) 356; A. Bernstein et al., Nucl. Inst. and Meth. A336 (1993) 23.

[8] J. Andruszków et al., DESY 92-066 (1992).

[9] F. Jacquet and A. Blondel, in Proceedings of the study for an ep facility in Europe 79/48 (1979) 391, ed. U. Amaldi.

[10] H1 Collab., H. Ahmed et al., Phys. Lett. B299 (1993) 374.

[11] ZEUS Collab., M. Derrick et al., DESY 94-32, acc. for publication by Z. Phys.

[12] A. Donnachie and P. V. Landshoff, Nucl. Phys. B244 (1984) 322;
P. V. Landshoff, Nucl. Phys. B (Proc. Suppl.) 18C (1990) 211.

[13] H. Abramowicz, E. M. Levin, A. Levy and U. Maor, Phys. Lett. B269 (1991) 613.

[14] M. Drees and F. Halzen, Phys. Rev. Lett. 61 (1988) 275;
R. Ghandi and I. Sarcevic, Phys. Rev. D44 (1991) R10;
J. R. Forshaw and J. K. Storrow, Phys. Rev. Lett. B268 (1991) 116;
R. S. Fletcher, T. K. Gaisser and F. Halzen, Phys. Rev. D45 (1992) 377.

[15] J. J. Sakurai, Phys. Rev. Lett. 22 (1969) 981.

[16] ZEUS Collab., M Derrick et al., "Measurement of the Elastic $\rho^o$ Photoproduction Cross Section at HERA", Subm. to the $27^{th}$ Int. Conf. on High Energy Physics, Glasgow 1994, Ref. 688.

[17] J. N. Lim, "Cross Section Measurement of the process $ep \rightarrow ep\,J/\psi$ at HERA", Talk given at the 27th Int. Conf. on High Energy Physics, Glasgow 1994.

[18] H1 Collab. H. Ahmed et al., "Photoproduction of $J/\psi$ mesons at HERA", DESY 94-153, subm. to Phys. Lett.

[19] ZEUS Collab., M. Derrick et. al., "Measurement of the Two-jet Cross Sections in Photoproduction at HERA", Subm. to the $27^{th}$ Int. Conf. on High Energy Physics, Glasgow 1994, Ref. 682.



[20] T. Greenshaw, M. Hapke, R. Prosi and K. Müller, "New Results from the H1 Experiment at HERA on Jets, the Proton Structure Function, Rapidity Gap Events, Charged Current Cross Section and Searches for New Particles", DESY 91-112.

[21] M. Glück, E. Reya and A. Vogt, Phys. Rev. D47 (1993) 867.

[22] H. Abramowicz, K. Charchula and A. Levy, Phys. Lett. B269 (1991) 458.

[23] W. D. Dau, "Structure Function $F_2$ from Deep Inelastic Electron-Proton Scattering at HERA", these Proceedings.

[24] H1 Collab., I. Abt et. al., Nucl. Phys. B407 (1993) 515;
ZEUS Collab., M. Derrick et al., Phys. Lett. B316 (1993) 412.

[25] H1 Collab., T. Ahmed et al., DESY 94-12, subm. to Phys. Lett. B.

[26] D. Haidt and H. Pietschmann: Landolt-Börnstein New Series I/10, Springer (1988).

[27] G. Ingelman, Proc. of the Workshop on Physics at HERA, Vol. 3 (1991) 1366, ed. W. Buchmüller and G. Ingelman;
M. Bengtsson, G. Ingelman and T. Sjöstrand, Nucl. Phys. B301 (1988) 554.

[28] ZEUS Collab., M. Derrick et al., Phys. Lett. B306 (1993) 158.

[29] H1 Collab., I. Abt et al., Z. Phys. C61 (1994) 59.

[30] D. Graudenz, Projet 3.6, to be publ.

[31] T. Brodkorb, E. Mirkes, University of Wisconsin Preprint, MAD-PH-821 (April 1994).

[32] S. Söldner-Remboldt, "Two-Jet Production in Deep Inelastic ep Scattering at HERA", Talk given at the $27^{th}$ Int. Conf. on High Energy Phys., Glasgow 1994.

[33] S. Bethke, Lectures given at the Scottish Universities Summer School, St. Andrews, Scotland, August 1-21, Heidelberg Preprint HD-PY 93/7.

[34] ZEUS Collab., M. Derrick et al., Phys. Lett. B315 (1993) 481.

[35] H1 Collab., T. Ahmed et al., DESY 94-133.

[36] L. Lönnblad, Lund preprint, LU TP-89-10;
L. Lönnblad, Comp. Phys. Comm. 71(1992) 15.

[37] P. Bruni and G. Ingelman, DESY 93-187, Proc. of the Europhysics Conf., Marseille (1993).

[38] ZEUS Collab., M. Derrick et al., Phys. Lett. B332 (1994) 228.